HAREM experiment data suggest a new line of research for fisheries management and the survey of marine surface life, in particular, for cetaceans and pelagic fish. Aiborne SAR could be more effective than any other monitoring technique, considering the large covered area, the noninfluence of clouds and the independence of the method facing of the fishery context. Now a large body of data on the geometric properties and radiometric signatures of these surface features should be collected during future aerial experiments and satellite simulations or actual satellite acquisitions (ERS 1), under a variety of wind, surface wave, and radar illumination and spectral band conditions. The next step is to improve the knowledge of the relationship between the schools' or nets' density and the radar image clues which would lead to conversion of schools or nets sensing into, respectively, abundance or fishing effort estimates, one of the major goals in halieutic surveys.

References

[1] M. Petit, J. M. Stretta, H. Farrugio, and A. Wadsworth, Etudes et thèses (Collection ORSTOM, 1990).
[2] W. Alpers, *Nature* vol. 314, pp. 245–247, 1985.
[3] J. P. Ford, J. B. Cimino, and C. Elachi, JPL Publication 82–95, 1983.
[4] B. A. Huges and J. F. R. Gower, *J. Geophys. Res.*, vol. 88, pp. 1809–1824, 1983.
[5] B. A. Huges, *J. Geophys. Res.*, vol. 83, pp. 455–465, 1978.
[6] R. F. Gasparovic, J. R. Apel, A. Brandt, and E. S. Kasischke, Tech. Digest. 6, 4, pp. 338–345, Johns Hopkins University Applied Physics Laboratory, 1986.
[7] M. Petit and J. M. Stretta, Collective vol. SCRS/88/32, 30, pp. 488–490, Int. Commission for the Conservation of Atlantic Tunas, 1989.
[8] R. Horn, *Proc. of IGARSS*, 1988.
[9] M. Petit, J. M. Stretta, and C. Dupouy, Doc. Tech. 302, pp. 127–140, FAO, 1989.
[10] J. F. Caddy and G. P. Bazigos, Doc. Tech. 257, FAO, 1985.
[11] A. Wadsworth, Doc. Tech. GDTA, Dec. 1986 Groupement pour le Développement de la Télédétection Aérospatiale, Toulouse, 1986.

SAR Ocean Image Representation Using Wavelets

Joseph G. Teti, Jr. and H. N. Kritikos

Abstract— **The utility of wavelet analysis as a tool for geophysical research is examined using both continuous and discrete versions of the wavelet transform. In both cases, waveform decomposition and reconstruction is possible using somewhat different computational procedures. The theoretical background of each procedure is briefly described and applied using a specific "wavelet." The wavelet used is based on a Gaussian function, and provides simultaneous time-frequency (or space-wavenumber) localization that meets the lower limit of the uncertainty principle. A representation of this type is ideally suited for the analysis of waveforms that arise from nonstationary processes. The properties of wavelet analysis are examined by expanding an FM-chirp waveform, and azimuth cuts taken from two different SAR ocean images. The performance and ease of implementation are compared for the continuous and discrete formulations, and the effects of filtering in wavelet phase space using the discrete case are also examined.**

Manuscript received July 26, 1991; revised January 22, 1992; rerevised March 12, 1992.

J. G. Teti, Jr. was with the Microwave Technology Division, Naval Air Warfare Center, Aircraft Division, Warminster, PA 18974. He is currently with JJM Systems, Inc., Ivyland, PA 18974.

H. N. Kritikos is with the Moore School of Electrical Engineering, University of Pennsylvania, Philadelphia, PA 19104.

IEEE Log Number 9200755.

I. Introduction

THE wavelet concept was first introduced to the engineering community by Morlet [7] for use in the representation of seismic data. Recently, the underlying theory has been formalized primarily by Daubechies [3]. A number of researchers have recently exposed many of the properties and potential applications for wavelet analysis [2], [5], [9]. The continuous wavelet transform can impose some troublesome characteristics for many applications, some of which are examined here. The discrete wavelet transform overcomes many of the shortcomings of the continuous version, however, the reconstruction algorithms are quite different.

Through the use of the "frame" concept Daubechies has developed a generalized theory which encompasses the discrete versions of both the Weyl–Heisenberg and the affine or wavelet cases of waveform representation [3]. A subset of each of these cases involves a decomposition and reconstruction on frames which are formulated with simultaneous time-frequency (space-wavenumber) localization. The advantages of decomposition and reconstruction with both time and frequency localization have been of interest to the remote sensing community for quite some time. Such examples include transient analysis of lightning [6], analysis of seismic data [7], SAR ocean image decomposition and filtered reconstruction for speckle reduction and feature extraction [8], etc. The condition of time-frequency localization in the Weyl–Heisenberg case results in the Gabor expansion which has been discussed in [2], [3], and further investigated and applied in [8]. The Gabor expansion uses a set of translated and modulated Gaussian functions as its frame, and produces a uniformly spaced lattice in phase space [3], [8]. The condition of time-frequency localization in the affine or wavelet case results in a wavelet expansion which uses Morlet's wavelet [3], [7]. Morlet's wavelet is also based on a Gaussian and was the result of extending Gabor's basic idea for more efficient representation of seismic data [7]. The corresponding wavelet expansion uses a set of translated and dilated (or contracted) modulated Gaussian functions as its frame, and produces a phase space lattice which is log-uniform in time and logarithmic in frequency. The details of this phase space are discussed in [3] and are also presented here. An analysis tool having the properties described can provide a numerically efficient representation of many types of geophysical phenomena. Also of interest in this work is the filtered reconstruction of SAR ocean image features through the use of the phase space information associated with the discrete wavelet transform. The format of this paper closely follows [8], and the subject waveforms studied here are the same as those studied in [8] to allow direct comparison. To appreciate the use of the discrete wavelet transform, some knowledge of frames is required and a brief development is presented. A more detailed discussion on frames is given by Young [10].

II. Theoretical Preliminaries

A. The Continuous Wavelet Transform

For finite energy functions $f \in L^2(\boldsymbol{R})$, the continuous wavelet transform F proposed by Morlet [7] is defined as

$$F(a,b) = \frac{1}{\sqrt{|a|}} \int_{-\infty}^{\infty} g^* \left(\frac{x-b}{a} \right) f(x)\, dx \tag{1}$$

where $g^*(x)$ is the complex conjugate of a particular wavelet "mother" function $g(x)$, and $(a,b) \in \boldsymbol{R}, a \neq 0$. The form of the wavelet transform is called continuous because the dilation and

translation scale space parameters (a, b) vary continuously. The wavelets are defined by translating and dilating the function $g(x)$ as

$$g_{ab}(x) = \frac{1}{\sqrt{|a|}} g\left(\frac{x-b}{a}\right). \tag{2}$$

To recover f from its wavelet transform the mother function $g(x)$ must satisfy the admissibility condition

$$c_g = 2\pi \int_{-\infty}^{\infty} dk\, |k|^{-1} |\hat{g}(k)|^2 < \infty \tag{3}$$

where $\hat{g}(k) = \frac{1}{\sqrt{2\pi}} \int_{-\infty}^{\infty} g(x) e^{ikx}\, dx$ is the Fourier transform of $g(x)$. The condition also implicitly requires that $g(x)$ have zero mean [2]. Using (3) with (1) the waveform f can be reconstructed from its wavelet transform by

$$f(x) = \frac{1}{c_g} \int\int F(a,b) \frac{1}{\sqrt{|a|}} g\left(\frac{x-b}{a}\right) \frac{da\, db}{a^2}. \tag{4}$$

From (4) it is clear that the continuous wavelet transform is straightforward to use, but it will be shown to be computationally intensive and difficult to apply in some situations. This will be discussed further in later sections.

B. The Discrete Wavelet Transform

To properly address the discrete wavelet transform the concept of a "frame" must be introduced. A sequence $\{\psi_n; n \in J$, a denumerable set$\}$ in $L^2(\boldsymbol{R})$ defines a frame if there exists numbers $A, B > 0$ such that

$$\forall f \in L^2(\boldsymbol{R}), \qquad A\|f\|^2 \le \sum_n |\langle \psi_n, f \rangle|^2 \le B\|f\|^2 \tag{5}$$

where A, B are called the frame bounds. If $A = B$ the frame is tight, if $A \approx B$ the frame is said to be snug. The frame definition given by (5) may be expressed for unit norm functions as

$$A\mathbb{1} \le \mathbb{T} \le B\mathbb{1} \tag{6}$$

where $\mathbb{1}$ is the identity operator, and the operator $\mathbb{T}$ is given by

$$\mathbb{T} = \sum_{n=-\infty}^{\infty} \psi_n \langle \psi_n, \bullet \rangle. \tag{7}$$

Since $A, B > 0$, the inverse of the $\mathbb{T}$ operator exists and satisfies the relation

$$\frac{1}{B}\mathbb{1} \le (\mathbb{T})^{-1} \le \frac{1}{A}\mathbb{1}. \tag{8}$$

Therefore, it then follows that functions $\{\tilde{\psi}_n\}$ may be defined as

$$\tilde{\psi}_n \triangleq \mathbb{T}^{-1} \psi_n \tag{9}$$

and constitute a "dual" frame with frame bounds $A^{-1}, B^{-1} > 0$. With $\{\tilde{\psi}_n\}$ and $\{\psi_n\}$ then

$$\forall f \in L^2(\boldsymbol{R}), \qquad f = \sum_n \tilde{\psi}_n \langle \psi_n, f \rangle. \tag{10}$$

To use (10) it is necessary to acquire the dual frame which from (6) can be found with the series

$$\tilde{\psi}_n = \frac{2}{A+B} \sum_{k=0}^{\infty} \left(\mathbb{1} - \frac{2}{A+B}\mathbb{T}\right)^k \psi_n \tag{11}$$

along with good estimates of the frame bounds A and B [1], [3]. The series in (11) is guaranteed to converge by virtue of its development and the tighter the frame the faster the convergence.

The phase space indices defined by the wavelet parameters (a, b) may be discretized for frame representation by choosing the dilation parameter $a = \pm a_o^m, a_o > 1$ and translation parameter $b = nb_o a_o^m$, where here $J = \{(m, n); m, n \in Z$, the set of integers$\}$. There is considerable flexibility in the selection of the lattice parameters (a_o, b_o), but a judicious choice can simplify implementation. The corresponding family of discretely labeled wavelets are given by

$$g_{mn}^{\pm}(x) = a_0^{-\frac{m}{2}} g(\pm a_o^{-m} x - nb_o). \tag{12}$$

In order to make use of (10), the dual frame in (11) must be determined. The ease at which this can be done depends upon the snugness of the frame. To provide an additional parameter to adjust the snugness of the frame while maintaining good time-frequency resolution, the concept of "voices" must be introduced [3], [7]. Thus, several wavelet mother functions $\{g^{\lambda}(x); \lambda = 0, \ldots, N-1\}$ where N is the total number of voices are needed for application. In practice, the mother functions are chosen to be related through dilation and are given by

$$g^{\lambda}(x) = a_o^{-\frac{\lambda}{N}} g(a_o^{-\frac{\lambda}{N}} x), \qquad \lambda = 0, \ldots, N-1. \tag{13}$$

The choice of N affects the density of the phase space lattice since the final lattice becomes the superposition of N lattices (i.e., one for each mother function).

Note that unlike the original frame, a single dual frame mother function does not exist in the same sense. The dual frame elements cannot be generated by translates and dilates of a single (or N) mother function(s) because the $\mathbb{T}$ operator defined by (7) does not commute with the translation operation in (12) [3], [5]. Construction of the dual frame elements requires a great deal of computational overhead unless the frame is extremely snug, and (11) can be approximated with only the $k = 0$ term.

C. The Morlet Wavelet and Discrete Phase Space

For both the continuous and discrete analyses, Morlet's wavelet is used to realize time-frequency localization that meets the lower limit of the uncertainty principle. The mother wavelet is the modulated Gaussian given by

$$g(x) = \pi^{-\frac{1}{4}} (e^{-i\nu x} - e^{-\frac{\nu^2}{2}}) e^{-\frac{x^2}{2}} \tag{14}$$

where $\nu = \pi\sqrt{\frac{2}{\ln 2}}$. Application of the discrete wavelet transform requires additional information about the frame. Daubechies [3] has estimated the frame bounds A and B quite accurately for a range of lattice parameters (a_o, b_o) and number of voices N, from which the values $(a_o, b_o) = (2, 1)$ and $N = 4$ have been selected for use here. These parameters with (14) result in an extremely snug frame with frame bounds $A = 6.918$ and $B = 6.923$ [3], i.e., $A \approx B$, and the dual frame is extremely well approximated by the $k = 0$ term in (11).

The phase space lattice for $N = 4$ voices is shown in Fig. 1. Note the decrease in time sample spacing for increasing frequency in packets of $N = 4$. Fig. 1 illustrates that wavelet analysis is not DC-coupled; i.e., no waveform information is mapped precisely centered around DC.

D. FM Chirp Waveform

The continuous wavelet transform representation of a pulse modulated FM-chirp waveform is shown in Fig. 2. Fig. 2(a) shows the original DC-coupled waveform superimposed over the reconstructed waveform. Notice the DC bias in the reconstruction resulting from the DC present in the original waveform. If the DC is removed from the original waveform the bias in the reconstruction essentially vanishes, as shown in Fig. 2(b). For both reconstructions the scale space parameters are varied in a pseudocontinuous fashion as $\{0.15 \le a \le 75; \delta a = 0.15\}$ and $\{-30 \le b \le 30; \delta b = 1.0\}$. Each

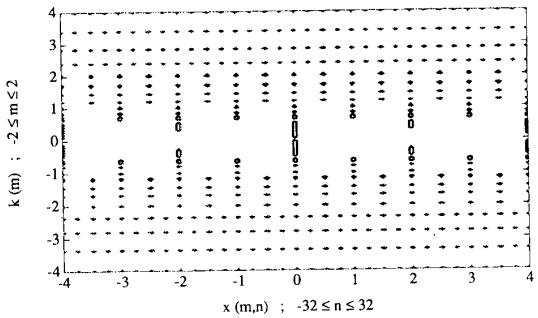

Fig. 1. Discrete phase space lattice for $N = 4$ voices where $k(m) = \pm a_o^{-m}$ and $x(m, n) = nb_o a_o^m$.

reconstruction uses 30 500 terms and for the result in Fig. 2(b), 99.74% of the original waveform power is recovered. Fig. 2(c) shows the corresponding scale space signature. The differences in the reconstruction performance between Figs. 2(a) and (b) show the sensitivity of continuous wavelet analysis to recovering DC even for the large range and high resolution of the phase space parameters used. Consequently, further continuous analysis will only be applied to "DC-removed" waveforms.

The discrete wavelet transform representation is now applied to the same DC-coupled pulse modulated FM-chirp waveform shown in Fig. 2(a). Fig. 3(a) shows the reconstructed waveform and illustrates that the DC present in the original waveform poses no trouble for the discrete analysis to recover. The discrete reconstruction uses $\{-2 \leq m \leq 11, -18 \leq n \leq 18\}$ (4144 terms) to yield 99.92% of the original waveform power. Less terms are permissive for good reconstruction. Fig. 3(b) shows the discrete wavelet phase space representation of this waveform illustrating the dominant coefficients produced by the inner product in (10).

III. SAR Ocean Image Representation

In this section, wavelet analysis is used for the representation of azimuth cuts taken from two different SAR ocean images. The azimuth cuts used are the same as those analyzed in [8]. The first azimuth cut is taken across a ship target of opportunity observed in an X-band image formed from data collected at VV polarization. The second azimuth cut is taken across a ship wake torn from conflicting velocity fields observed in a C-band image formed at VV polarization.

A. Continuous Wavelet Analysis

The ship image azimuth cut selected is shown in Fig. 4(a) with the DC content removed, and Fig. 4(b) shows the continuous reconstruction. The scale space parameters used for the reconstruction are varied over the reduced range in a pseudocontinuous fashion as $\{0.15 \leq a \leq 30; \delta a = 0.15\}$ and $\{-10 \leq b \leq 10; \delta b = 1.0\}$. The reconstruction uses 4200 terms to recover 90.35% of the original waveform power. The performance of the reconstruction is primarily limited by the high frequency cut off associated with the sampling rate and dilation parameter which causes aliasing. Increasing the range of the scale space parameters without increasing the translation parameter resolution δb, and accordingly the ordinate axis resolution (0.1 is used) of the waveform, quickly destabilizes the reconstruction. The instability is believed to be caused by the difficulty in approximating the integrations at fine scales through both the decomposition and reconstruction which requires smaller δb. A better reconstruction was not pursued because it would require increasing the number of terms well beyond the 4200 terms used. The

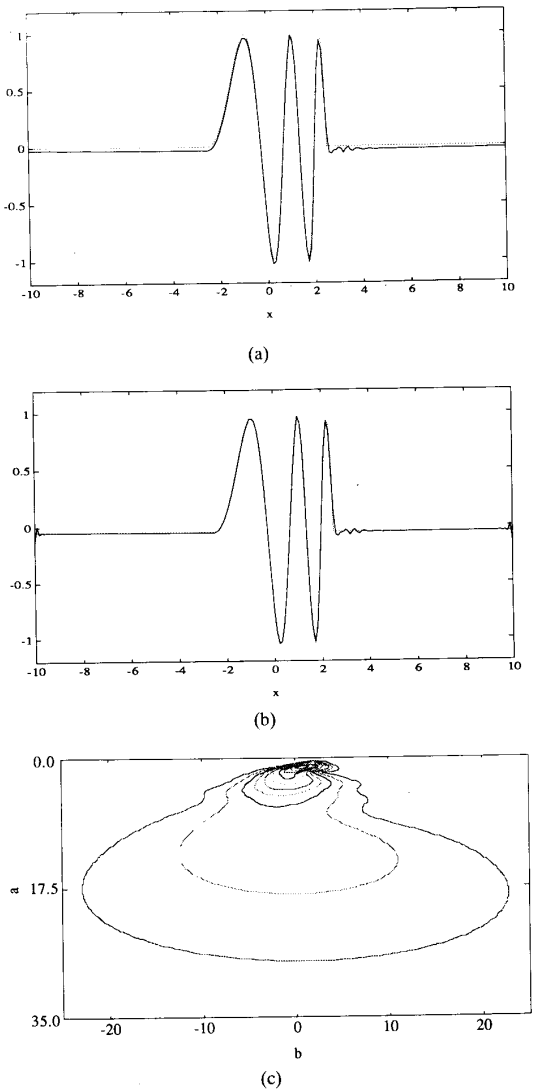

Fig. 2. (a) Original (- - -) and reconstructed (—) DC- coupled FM-chirp waveform. (b) Original (- - -) and reconstructed (—) DC-removed FM-chirp waveform. (c) Continuous scale space contour for the reconstruction in 2(b).

sensitivity of the reconstruction performance to the characteristics of the scale space parameters and the subject waveform's resolution and frequency content is further illustrated by the continuous analysis of the ship wake SAR image azimuth cut.

Fig. 5(a) shows the original DC-removed ship wake image azimuth cut and Fig. 5(b) shows the continuous reconstruction. The characteristics of the phase space parameters are the same as those used for the ship image azimuth cut reconstruction in Fig. 4(b). The reconstruction for ship wake azimuth cut is highly unstable for the reasons previously discussed. It is conjectured that there is additional aliasing responsible for the relative degradation in the reconstruction of Figs. 4(b) and 5(b) because of additional high frequency information present in the ship wake image azimuth cut (compare Figs. 4(a) and 5(a)).

B. Discrete Wavelet Analysis

The discrete wavelet reconstruction of the original ship image azimuth cut shown in Fig. 4(a) with the DC content removed is shown in Fig. 6(a) (superimposed as a dotted line over the original)

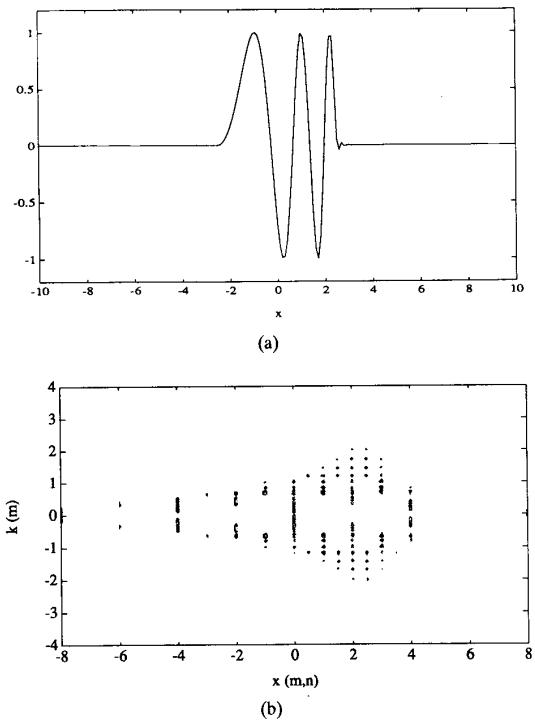

Fig. 3. (a) Reconstructed FM-chirp waveform (discrete analysis). (b) Wavelet phase space contour for the reconstruction in (a).

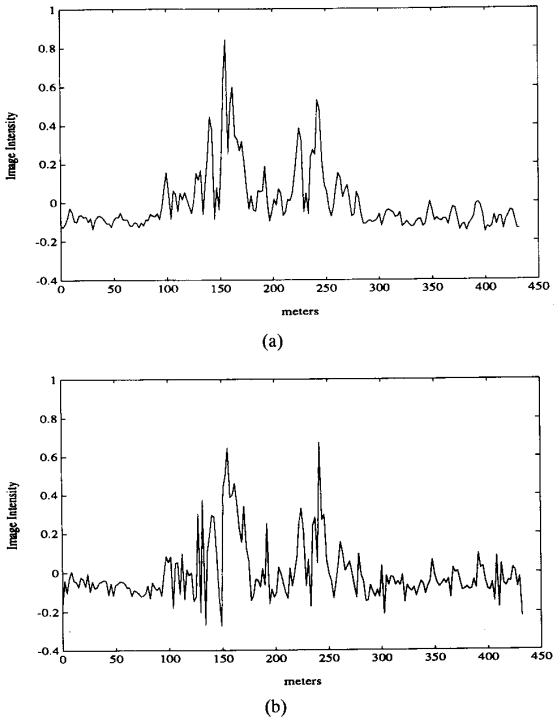

Fig. 4. (a) Original SAR ship image azimuth cut. (b) Reconstructed SAR ship image azimuth cut (continuous analysis).

for the parameters given in Section II.C. The reconstructed waveform is nearly identical and uses $\{-2 \leq m \leq 12, -20 \leq n \leq 20\}$ (4920 terms) to recover 97.21% of the power. Fig. 6(b) shows a subsection of the corresponding phase space signature, illustrating the localization of the dominant coefficients produced by the inner product in (10).

Similarly, the discrete wavelet reconstruction of the original ship wake image azimuth cut from Fig. 5(a) is shown in Fig. 7(a) (superimposed as a dotted line over the original) for the parameters given in Section II.C. The reconstructed waveform is of very good quality and uses $\{-2 \leq m \leq 12, -40 \leq n \leq 40\}$ (9720 terms) to yield 90.12% of the original power. Note that in this case, the azimuth cut expanded is twice the length of the ship azimuth cut, and accounts for the relatively larger number of terms used in the reconstruction. Fig. 7(b) shows a subsection of the corresponding phase space signature, illustrating the localization of the dominant coefficients produced by the inner product in (10).

C. Filtered Reconstruction Using Discrete Wavelet Analysis

Unlike continuous wavelet analysis, discrete wavelet analysis can be readily used for filtering purposes. This can be realized through limiting the reconstruction to only include dominant frame contributions from the inner product in (10). Note that since wavelet analysis is not DC coupled, low pass filtering does not apply. Filtering can only be band pass with an extremely low frequency cut off possible. Referring to Fig. 6, two filtered image cuts of the ship response have been constructed and are shown in Fig. 8. A narrowband response and a more detailed wideband response are shown superimposed over the original reconstruction from Fig. 6(a). The narrowband filtered cut uses 200 terms and represents 52.60% of the original waveform power, and the more detailed filtered cut uses 320 terms and represents 65.23% of the original waveform power. Note that the ship scattering envelope is preserved in both cases.

Referring to Fig. 7, two filtered image cuts of the ship wake response have been constructed and are shown in Fig. 9. A narrowband response and a more detailed wideband response are shown superimposed over the original reconstruction from Fig. 7(a). The narrowband filtered cut uses 1512 terms and represents 65.47% of the original waveform power, and the more detailed filtered cut uses 2016 terms and represents 81.58% of the original waveform power. Similar to the filtered ship image azimuth cuts, the scattering envelope of the ship wake is preserved in both cases.

IV. Conclusions

The utility of wavelet analysis for SAR ocean image representation has been examined using both continuous and discrete versions of the wavelet transform. The theoretical background of each procedure was briefly described and applied using a modulated gaussian mother wavelet to provide time-frequency (or space-wavenumber) localization that meets the lower of the uncertainty principle. The properties of each formulation have been examined by expanding an FM-chirp waveform, and azimuth cuts taken from two different SAR ocean images.

The performance in reconstructing the FM chirp waveform illustrated the sensitivity of the continuous analysis to recover the DC content of the subject waveform. The discrete analysis did not have difficulty recovering DC information. Consequently, the subsequent continuous analysis performed on SAR ocean image azimuth cuts was only applied to the DC-removed version of the waveforms. Additional difficulties were encountered in the appropriate selection of the pseudocontinuous phase space parameters. The SAR ocean image

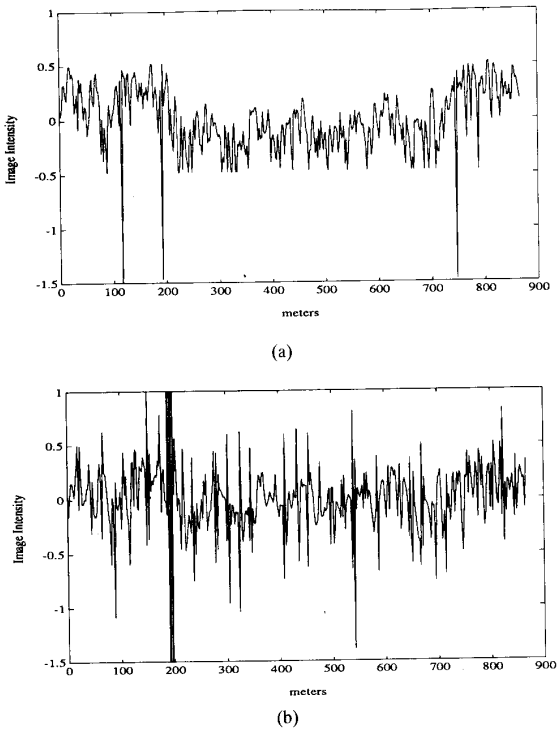

Fig. 5. (a) Original SAR ship wake image azimuth cut. (b) Reconstructed SAR ship wake image azimuth cut (continuous analysis).

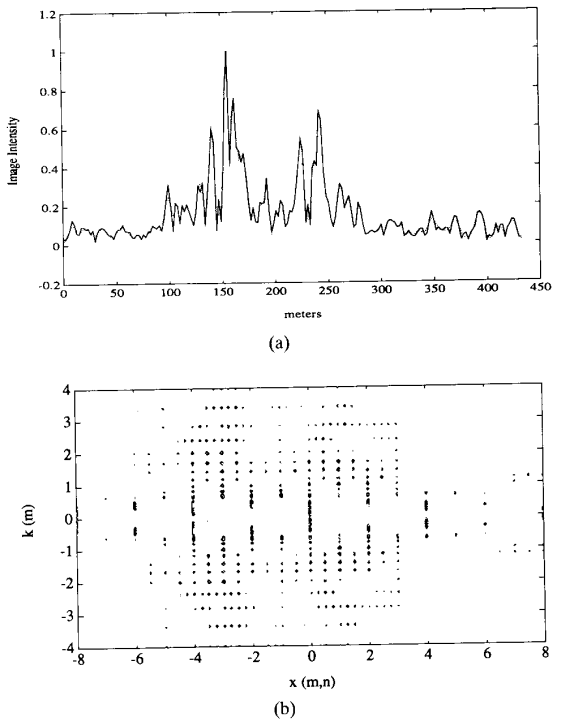

Fig. 6. (a) Reconstructed SAR ship image azimuth cut (discrete analysis). (b) Phase space contour for the reconstruction in (a).

cut reconstructions for the continuous analysis show signs of aliasing which resulted from the combination of the subject waveform's high frequency content and the resolution of the continuous reconstruction parameters. Here again, the discrete formulation did not encounter the same difficulties and extremely stable and high quality reconstructions were realized. Note that a significant computational difficulty in performing the discrete analysis was avoided by the selection of an extremely snug frame. The snug frame allowed the dual frame elements from (10) to be approximated by the $k = 0$ term.

The phase space signature provided by the discrete wavelet analysis proved to be very useful for performing filtering. The reconstruction uses a unique phase space signature which is localized at the lattice points (time, frequency) $= (nb_o a_o^m, \pm a_o^{-m})$ for each voice. With the reconstruction being limited to dominant frame contributions, filtering is performed which gracefully reduces high frequency information while still preserving image features. This has been clearly shown for the SAR image cuts that have been analyzed. The filtering is successful at removing speckle while still preserving the scattering envelope of the ship and wake features. This property is a consequence of the time or space translation step being smaller for higher frequencies (corresponding to $m \ll 0$), and allows discrete wavelet analysis to zoom in on sharp edges or discontinuities (singularities) that may be present. Continuous wavelet analysis also possesses the same properties but they are much more difficult to exploit for application. The continuous analysis phase space signature does not allow filtering to be easily performed.

This work has exposed many of the properties of wavelet analysis and in particular the usefulness of the discrete wavelet transform for geophysical research. The affine or wavelet coherent frame used here along with the Weyl–Heisenberg coherent frame applied in [8]

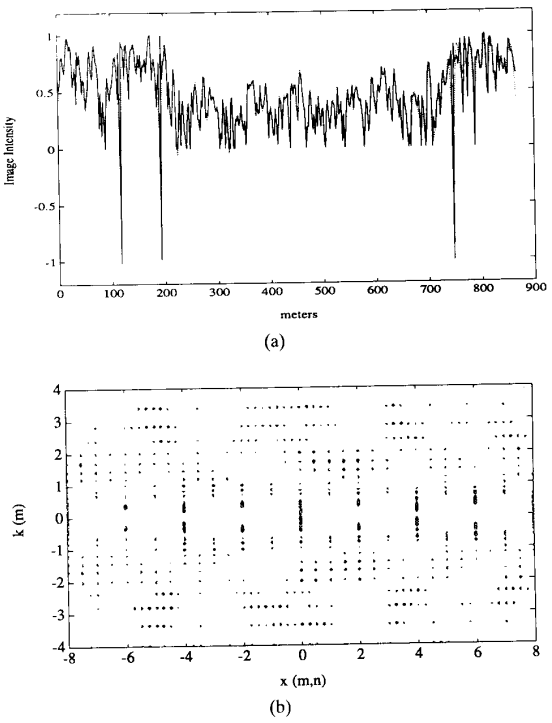

Fig. 7. (a) Reconstructed SAR ship wake image azimuth cut (discrete analysis). (b) Phase space contour for the reconstruction in (a).

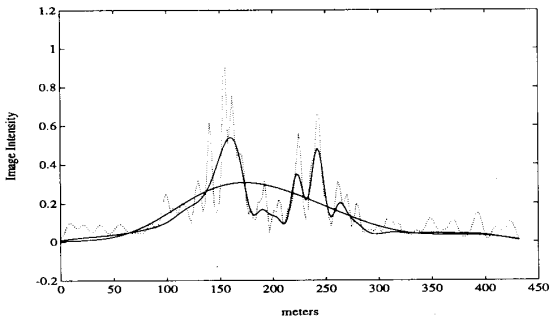

Fig. 8. Filtered SAR ship image azimuth cuts (see text).

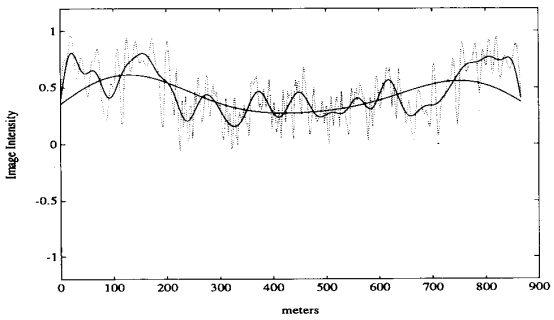

Fig. 9. Filtered SAR ship wake image azimuth cuts (see text).

together make up a pair of numerically tractable and robust analysis tools for nonstationary processes. High level applications utilizing both types of coherent frames for feature extraction and identification are interest areas of future research.

ACKNOWLEDGMENT

The authors sincerely appreciate the helpful comments and suggestions of the anonymous reviewers which have improved the manuscript.

REFERENCES

[1] R. J. Duffin and A. C. Schaeffer, "A class of nonharmonic Fourier series," *Trans. Am. Math Soc.,* vol. 72, pp. 341–366, Mar. 1952.
[2] J. M. Combes, A. Grossmann, and Ph. Tchamitchian, Eds., *Wavelets.* Berlin Heidelberg: Springer-Verlag, 1990.
[3] I. Daubechies, "The wavelet transform, time frequency localization, and signal analysis," *IEEE Trans. Inform. Theory,* vol. 36, pp. 961–1005, Sept. 1990.
[4] D. Gabor, "Theory of communication," *J. IEE (London),* vol. 93, no. 3, pp. 429–457, Nov. 1946.
[5] S. Mallat, "A theory for multiresolution signal decomposition," Ph.D. dissertation, University of Pennsylvania, Moore School of Electrical Engineering, 1988.
[6] V. Mazur, D. S. Zrnic, and W. D. Rust, "Lightning channel properties determined with a vertically pointing doppler radar," *J. Geophys. Res.,* vol. 90, no. D4, pp. 6165–6174, 1985.
[7] J. Morlet, G. Arens, E. Fourgeau, and D. Giard, "Wave propagation and sampling theory," *Geophys.,* vol. 47, no. 2, pp. 203–236, 1982.
[8] J. G. Teti, Jr. and H. N. Kritikos, "SAR ocean image decomposition using the Gabor expansion," *IEEE Trans. Geosci. Remote Sensing,* vol. 30, pp. 192–196, Jan. 1992.
[9] B. B. Wells, "Applications of wavelets to radar," *Proc. of Progress in Electromagnetics Research Symposium (PIERS),* 1991.
[10] R. M. Young, *An Introduction to the Fourier Series.* New York: Academic Press, 1980.

Thickness Profiling of Freshwater Ice Using a Millimeter-Wave FM-CW Radar

Norbert E. Yankielun, Steven A. Arcone, and Robert K. Crane

***Abstract*—A prototype broadband millimeter wave (26.5 to 40 GHz) FM-CW radar employing digital signal processing techniques has been developed for profiling the thickness of freshwater ice. The radar was tested at elevations of up to 7 m above ice surfaces and at speeds up to 40 km/h both from a surface vehicle and a helicopter. The thickness of pond and river ice sheets between 3 and 35 cm thick with and without fresh snow cover and minimal surface roughness showed direct correlation with borehole thickness measurements. Losses due to volume scattering by imbedded air bubbles did not significantly affect system capability to discern the air/ice and ice/water scattering boundaries.**

I. INTRODUCTION

Obtaining real-time, rapid and high resolution freshwater ice thickness profiles over large expanses of frozen freshwater bodies has wide application and utility. A device able to insure the safety of personnel and the ability of vehicles to traverse frozen bodies of water would have tactical, strategic, commercial, and recreational applications. Specifically, an ability to measure ice thickness in the range of 3 or more cm is addressed in this discussion.

There has been considerable effort placed on the development and application of radar for geophysical profiling of ground, sea ice and freshwater ice for at least the last 25 years as reviewed by Wills [1], Riek *et al.* [2], and Page and Ramseier [3]. The majority of the effort, to date, has been with impulse radar at frequencies less than 1 GHz with an ability to resolve ice thicknesses in the range of 10 to 20 cm [2]–[5]. Microwave approaches have also tried the impulse technique to reach about the same resolution [6]. As unsafe conditions occur generally at less than 10 cm, there is a need for higher resolution and therefore, a shorter pulse. Since impulse generation at mmw frequencies is not yet conveniently available, the spread spectrum technique of FM-CW is then investigated.

The FM-CW technique has been applied at X-band to measure freshwater ice thicknesses down to 14 or 15 cm [7], for geophysical remote sensing applications at 8 to 12 GHz [8] and for snow stratification investigations at 8 to 12 GHz [9], [10]. To date, no profiling radar measurements of ice thickness less than 10 cm have been reported. Here we discuss a prototype FM-CW radar operating in the 26.5–40 GHz frequency range that fulfills this task. Propagation in freshwater ice has not been found to be a limitation and scan generation at reasonable profiling speeds is possible with this technique.

Manuscript received April 22, 1991; revised January 8, 1992. Funding for this research project was provided by DA Project 4A161102AAT24 for the U.S. Army Corps of Engineers.

S. A. Arcone is with USA CRREL, Hanover, NH 03755.
N. E. Yankielun is with Dartmouth College, Hanover, NH 03755.
R. K. Crone is with the University of Oklahoma, Norman, OK 73019.
IEEE Log Number 9201496.